Preferred citation: V. Wallqvist, P.M. Claesson, A. Swerin, C. Östlund, J. Schoelkopf and P.A.C. Gane. Adhesive and long-range capillary forces between hydrophobic surfaces in water: effects of surface topography. In **Advances in Pulp and Paper Research, Oxford 2009**, *Trans. of the XIVth Fund. Res. Symp. Oxford, 2009*, (S.J. I'Anson, ed.), pp 1167–1191, FRC, Manchester, 2018. DOI: 10.15376/frc.2009.2.1167.

ADHESIVE AND LONG-RANGE CAPILLARY FORCES BETWEEN HYDROPHOBIC SURFACES IN WATER: EFFECTS OF SURFACE TOPOGRAPHY

Viveca Wallqvist[1], *Per M. Claesson*[1,2], *Agne Swerin*[1,*],
Catherine Östlund[3], *Joachim Schoelkopf*[4]
and Patrick A. C. Gane[4,5]

[1]YKI, Ytkemiska Institutet AB/Institute for Surface Chemistry, Box 5607, SE-114 86 Stockholm, Sweden
[2]Department of Chemistry, Surface and Corrosion Science, Royal Institute of Technology, SE-100 44 Stockholm, Sweden
[3]Innventia AB, Box 5604, SE-114 86 Stockholm, Sweden
[4]Omya Development AG, CH-4665 Oftringen, Switzerland
[5]Department of Forest Products Technology, Helsinki University of Technology, FI-02015 Helsinki, Finland

ABSTRACT

Interactions between a hydrophobic probe particle and surfaces with nanoscopic surface features have been investigated. Such surfaces were prepared by polishing or by spin-coating of nano-particles. The surface topography was characterized by AFM, using the methods of high-resolution imaging, low-resolution imaging using the probe particle, and by the rolling ball method. The polished surfaces display sharp nanoscopic peaks and hardly

---

*Corresponding author: Tel.: +46 768 640031. E-mail address: agne.swerin@yki.se

any crevices. In contrast, the spin-coated surfaces can be characterized as nanostructured, due to the high density of nanoparticles that on a short length scale provides a regular pattern of crevices and hills. On all surfaces a larger waviness is also distinguished. In all cases the dominant force at short separations was found to be a capillary attraction due to the formation of an air/vapour condensate. Our data show that the large-scale waviness of the surface does not significantly influence the range and magnitude of the capillary attraction, but large local variations in these quantities are found. The large variation in adhesion force corresponds to a small variation in local contact angle of the capillary condensate at the surfaces. The report discusses how the nature of the surface topographical features influences the capillary attraction by influencing the local contact angle and by pinning of the three-phase contact line. The effect is clearly dependent on whether the surface features exist in the form of crevices or as extending ridges.

Keywords: Surface forces, AFM, capillary force, hydrophobic interaction, surface roughness, surface topography, cavitation, bubbles

1. INTRODUCTION

The interactions between macroscopic non-polar surfaces in aqueous environments have been of great interest since Israelachvili and Pashley reported the presence of a long-range hydrophobic interaction between such surfaces [1]. It was early realised that cavitation occurred when two hydrophobic surfaces were brought into contact [2], but it took several years before it was suggested that cavitation or bridging bubbles could explain the long-range nature of the attractive force observed on bringing such surfaces together [3–5]. This mechanism seems to explain many, but not all, of the results reported in the literature [6], and the topic is still frequently discussed [7–12]. Recently, the complementarity of the attraction between non-polar surfaces in water to that between hydrophilic surfaces in (wet) air has been demonstrated, giving further credence to the idea that both are due to capillary condensation [12]. In the former case a capillary of gas/vapour gives rise to the force, and in the latter case a capillary condensate of water causes the attractive force. We note that surface roughness and chemical heterogeneity in some cases have been shown to have a more significant influence on the ultimate range of the attractive force between non-polar surfaces in water than the actual hydrophobicity as judged from contact angle measurements [13, 14]. Thus, the range and magnitude of the attraction can in general not be predicted by a measurement of the macroscopic contact angle.

Talc is a mineral frequently used in the pulp and papermaking industry for pitch control and as coating pigment. Talc surfaces are not as pure and smooth as the frequently used model surfaces, hydrophobized mica or silica. In our earlier reports [15],[16] we have shown that the long-range attraction between a talc surface and hydrophobic particles, pitch particles from paper mills as well as traditional silanized silica spheres, displays the characteristic features of forces induced by bridging bubbles/cavities. It was found that the range and magnitude of the attraction varied depending on the probe used and on the exact location on the talc surface. The variation is not only depending on the surfaces' hydrophobicity, as judged by contact angle measurements, but also on other factors where surface topography effects are hypothesized to play an important role. In this study we set out to explore this further by using rough surfaces with nanoscale topographical features in order to elucidate how such features affect the long-range attraction between non-polar surfaces in water. In order to mimic the roughness of real surfaces we have avoided making perfectly regular surface structures, but rather explored substrates that show roughness features over both the nanometer and micrometer length scale.

2. EXPERIMENTAL

2.1 Materials

Thermally oxidized silicon wafers purchased from Wafer Net, Germany, were used as substrates. They were either polished or spin-coated with silica nanoparticle solutions. Polishing was done with a Masterprep polishing suspension (Alumina 0.05 μm from Buehler Ltd, Lake Bluff, IL, USA). Silica, SiO_2, particles with brand name Bindzil 50/80 and Bindzil 30/360 from Eka Chemicals AB (Bohus, Sweden), were used for coating a macroscopic silica surface. The particle diameter of Bindzil 50/80 is 40 nm, whereas Bindzil 30/360 is smaller with a diameter of 9 nm.

The water used in all experiments and sample preparations was obtained from a Milli-Q Plus Unit (Millipore, Bedford, MA, USA) including ion exchange, active carbon adsorption and reverse osmosis prior to the final 0.22 μm filtration step. The water resistivity after this treatment was 18.2 Mohm cm. The water used for the AFM measurements was degassed prior to use by employing a water jet pump and a magnetic stirrer. NaCl p.a. was obtained from Merck, Germany and used as received. Ethanol, (99.7 vol-% pure) and acetone were obtained from Solveco, Sweden. The surfactant Berol 535 (technical grade penta(ethylene glycol) monoundecyl ether) used for dispersing the nanoparticles was obtained from AkzoNobel Surface Chemistry, Stenungsund, Sweden.

Colloidal silica particles with a radius, R, of 2.5 µm (Bangs Laboratories, Inc., USA) were used as probes for the force measurements. They, and the substrate surfaces, were rendered hydrophobic by the use of tridecafluoro-1,1,2,2 tetra hydro-octyl trichlorosilane (ABCR, Germany). A thermosetting glue (Epikote 1004, Resolution Europe B.V., The Netherlands) was used in the preparation of cantilevers and substrates for the AFM measurements.

2.2 Sample preparations

2.2.1 Silica surfaces

Silicon wafers with an oxide layer of about 100 nm thickness [17] were cut into a size of approximately 1 × 1 cm^2. They were cleaned by immersion in a solution of $H_2O/HCl/H_2O_2$ (66:21:13) at 80°C for 10 min, followed by rinsing extensively with Milli-Q water, and finally immersion in $H_2O/NH_3/H_2O_2$ (71:17:12) at 80°C for another 10 min. After rinsing with Milli-Q water, the surfaces were placed in ethanol until use.

2.2.2 Polished surfaces

Silica surfaces were mounted with double-sided tape on resin blocks. A disc with a polishing cloth (Chemomet I) was mounted in a grinding and polishing machine (Phoenix 4000) and wetted with water. Next, 5 cm^3 of the Masterprep suspension was added onto the polishing disc that was rotated with a speed of 100 min^{-1} using a force of 10 N. The sample area was approximately 100 mm^2. Different polishing times were selected in order to achieve different levels of surface modification. After polishing, the samples were thoroughly rinsed in Milli-Q water.

2.2.3 Nanoparticle coated surfaces

Robust nanoparticle coated surfaces were obtained by using combinations of tetraethoxysilane (TEOS) and silica nanoparticles. One solution was prepared by mixing 4 g of TEOS with 3 g of an aqueous HCl solution held at pH 2 in 25 g of ethanol. This solution was stirred for 30 min to complete the hydrolysis process. The second solution contained nanoparticles mixed with 2 wt% surfactant Berol 535 and Milli-Q water in the ratio 1:1:10. Dispersion of the nanoparticles was facilitated by employing an ultrasonic disintegrator (Sonyprep 150) for 2 min. The dispersed nanoparticles were then mixed with hydrolysed TEOS solution (2:1) and exposed to ultrasound in the ultrasonic disintegrator for another 2 min. This particle dispersion was applied to the silica surfaces by using a photo-resist spin-coater (PWM32, Headway Research, Inc., USA). The whole surface was coated with the solution before the spinning was started. The spin-coater was operated at 1500 min^{-1} for 30 s, and the acceleration and retardation times were set to 7.5 and 3.0 s, respectively. The coated silica surfaces were then dried in air and calcinated for 3 h at 550°C. The presence of TEOS in the nanoparticle dispersion facilitated attachment of the nanoparticles to each other and to the substrate, which resulted in a robust surface coating that was not affected by the force measurements.

2.2.4 Hydrophobised silica

Silica spheres were glued to calibrated cantilevers by using a small amount of Epikote 1004. The cantilevers were thereafter placed in a desiccator together with beakers containing some tridecafluoro-1,1,2,2 tetra hydro-octyl trichlorosilane for 20 h. After extensive rinsing with ethanol the cantilevers were dried before being used for force measurements. The polished as well as the nanoparticle covered silica surfaces were hydrophobised in a similar manner prior to force measurement. The water contact angle achieved was in the range 85–93°, which is slightly higher than the around 80° found for natural talc [15].

2.3 Methods

2.3.1 Force measurements

The forces acting between a hydrophobic probe and a substrate surface were measured using an AFM (Nanoscope III, Digital Instruments, USA) equipped with a liquid cell. The cantilevers (CSC12/tipless/No Al, Mikro-Masch, Estonia) were calibrated using the method proposed by Sader *et al.* [18]. Measurements were performed in aqueous 10 mM NaCl. During the AFM force measurements the trigger mode was set to “relative” and the trigger threshold was 100 nm. Relative trigger mode means that all force curves have the same preset maximum cantilever deflection relative to that at large surface separation (defined as zero deflection). A driving velocity of

400 nm s^{-1} was used for all measurements, which does not give rise to any significant hydrodynamic force [15].

2.3.2 Imaging

Images of the substrate surfaces were recorded with the same AFM instrument as employed for force measurements. High-resolution images in air were obtained in tapping mode using non-contact ultrasharp silicon cantilevers (NSCS12, NT-MDT, Russia). This provides information on the nanoscale structure of the surface layer. In addition, low-resolution images of the region used for force measurements were obtained, after force mapping, by imaging the surface with the probe itself. This imaging mode provides information on how the surface roughness is sensed by the probe. In addition, the high-resolution images were processed using the rolling-ball method, which has been applied in the paper industry for estimation of the pore volume at the interface between paper web and press felt [19]. The principle of the rolling-ball method is illustrated in Figure 1. Briefly, a ball with a given radius is used to delineate a surface of the topography data set. A smaller ball goes deeper into the valleys and experiences a rougher surface than a larger ball, i.e. the result is a convolution of the topography and the ball dimension.

2.3.3 Contact angles

Contact angles were measured using a dynamic contact angle and absorption tester (FibroDAT 1100, FibroSystems AB, Sweden), in which a drop of a specified volume is applied to a surface using an automated micro-pipette.

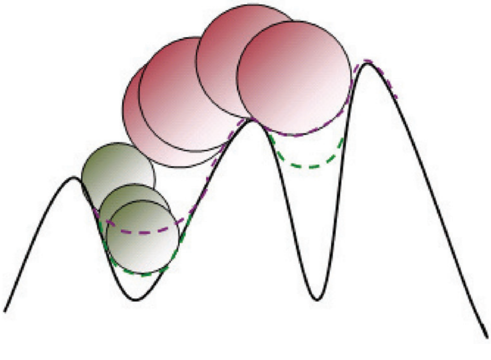

Figure 1. A schematic illustration of the rolling ball method. A smaller ball follows the surface topography closer than a larger ball.

The drop shape is captured with a high speed camera from the deposition time and the contact angle is calculated by the apparatus software as an average of the right and the left projected angles.

3. RESULTS

In this section we first discuss topography and surface interactions between the probe and the polished silica surfaces. We then proceed to the results obtained for the nanostructured surfaces obtained by spin-coating of silica nanoparticles.

3.1 Surface topography

The images displayed in Figure 2 illustrate the topography achieved by polishing the silica substrate for 2 s. Figure 2A shows the nanoscale features of the

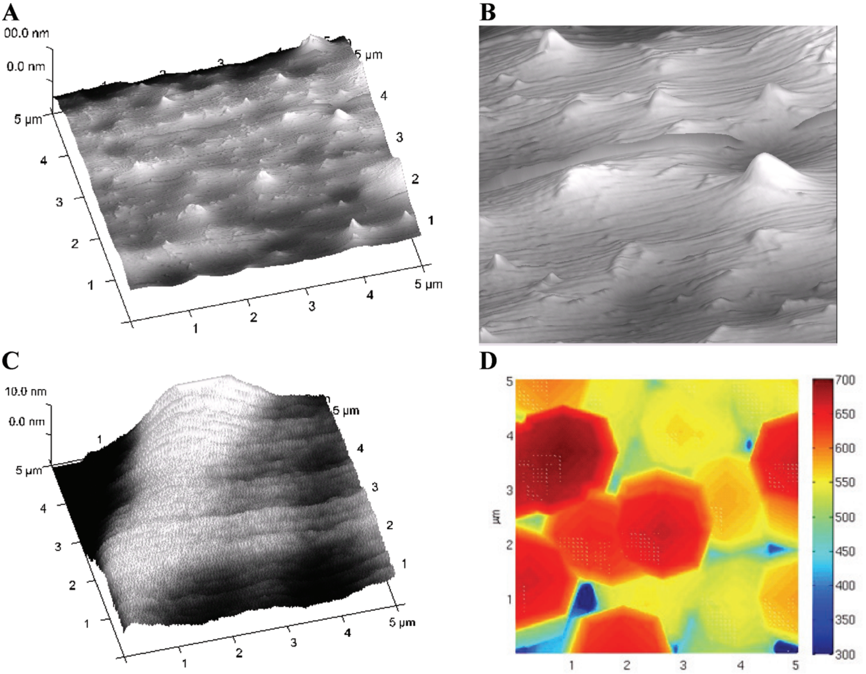

Figure 2. Surface polished 2 s. (A) High resolution 5 × 5 µm^2, (B) detail on the high resolution surface, (C) low resolution 5 × 5 µm^2 and (D) rolling ball image.

surface, but also a large-scale waviness. The local nanoscale roughness is more clearly illustrated in Figure 2B, where the sharp surface features are emphasized. Figure 2C, which is a low-resolution image obtained by using the colloidal probe as imaging tool, emphasizes the more large-scale wavy features of the surface layer. Finally, Figure 2D is constructed from Figure 2A using the rolling ball method with a ball radius of 2.5 µm, corresponding to the size of our probe. Clearly, similar structural features are observed by processing a high-resolution image with the rolling ball method as is obtained by imaging the surface with the colloidal probe. We note that the image in Figure 2C, and all other low-resolution images shown below, represents the surface structure of the region where surface forces have been measured. In contrast the high-resolution images in Figures 2A and 2B are obtained in a different surface region.

The corresponding high-resolution and low-resolution images of the silica surfaces after 10 s and 40 s of polishing are provided in Figures 3–4. For the surface polished for 40s there is also a rolling-ball image. We note that an increased polishing time results in a decrease in number of sharp surface features, compare Figures 2A, 3A and 4A, whereas the large-scale waviness remains largely unaffected. Note the similarity between the low-resolution images and the rolling-ball images reconstructed from the high-resolution AFM images. The roughness characteristics over a 5 × 5 µm^2 area on the different surfaces are presented in Table 1[i], which also includes data for the macroscopic water contact angle.

Table 1. Roughness characteristics and water contact angle of polished and silanized silica substrates.

Polishing time	*R_a (nm)*	*R_q (nm)*	*Water contact angle*
2 s	9.08	11.9	90°
10 s	4.56	6.62	86°
40 s	0.315	0.405	93°

[i]

$$R_q = \sqrt{\frac{\sum_{i=1}^{N}(Z_i - Z_{\text{ave}})^2}{N}}$$

Z_{ave} = average Z value within the given area
Z_i = local Z value
N = Number of points within the given area

$$R_a = \frac{\sum_{i=1}^{N} Z_i - Z_{ave}}{N}$$

Z_{ave} = Z value at the centre plane
Z_i = local Z value
N = number of points within the given area

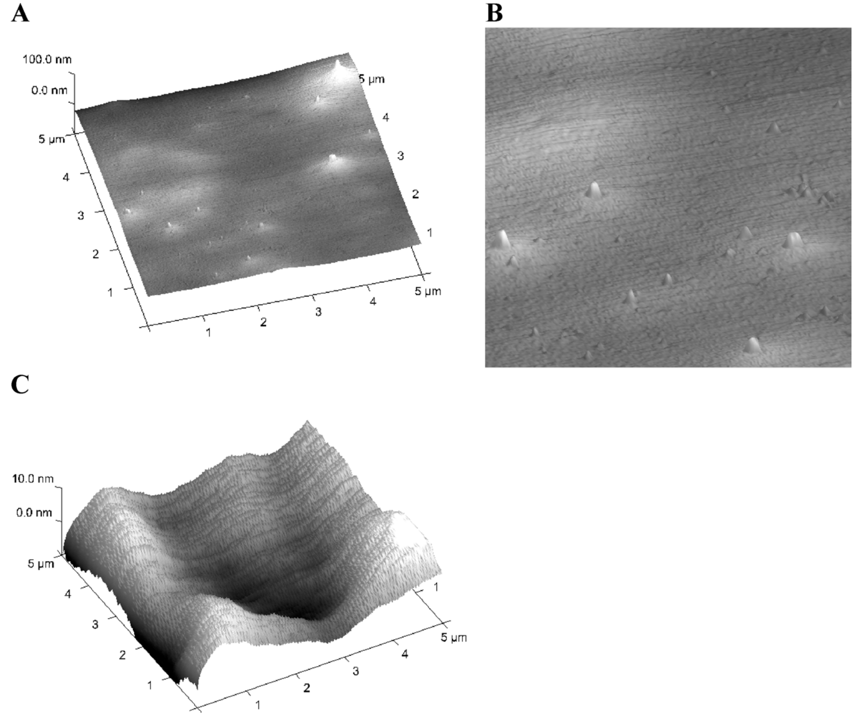

Figure 3. Surface polished 10 s (A) High resolution 5 × 5 μm^2, (B) 0.4 × 0.4 μm^2 detail on the high resolution surface and (C) low resolution 5 × 5 μm^2.

High-resolution and low-resolution images of surfaces covered with a spin-coated layer of 9 and 40 nm silica particles, respectively, are provided in Figures 5 and 6. The surface topography is characterized by a local nanostructure, with larger features for the surface with 40 nm particles than for that coated with 9 nm particles, and a wavy topography over larger length scales, as emphasized by the low-resolution image (Figures 5B and 6B).

The roughness characteristics of these surfaces are presented in Table 2. The macroscopic water contact angle on the two surfaces is also provided in Table 2. We note that the surface with the larger nanoparticles displays a slightly larger water contact angle than the one with smaller nanoparticles.

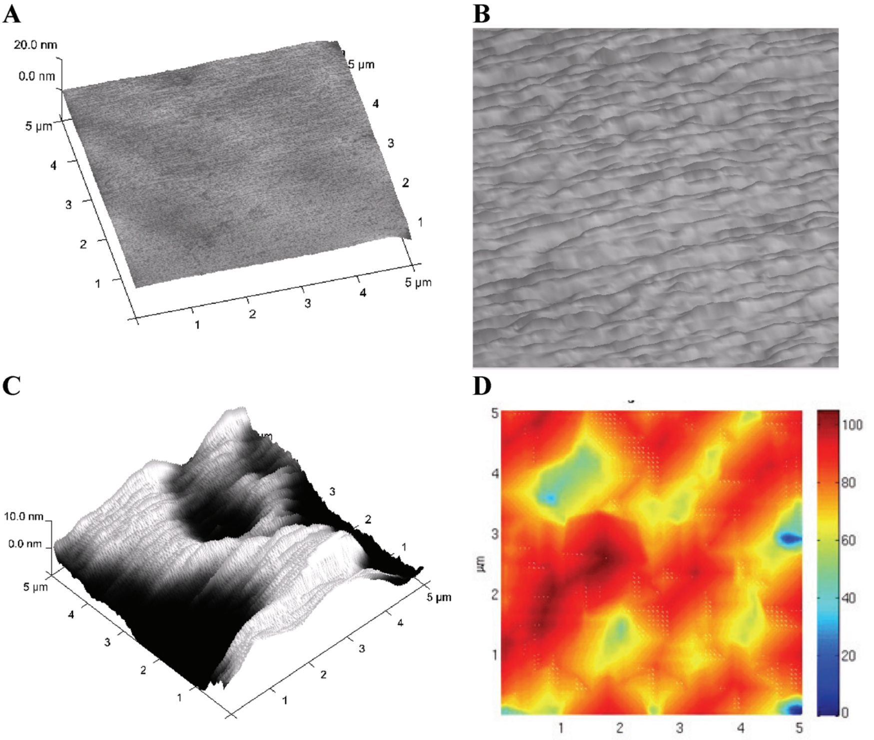

Figure 4. Surface polished 40 s. (A) High resolution 5 × 5 µm^2, (B) detail on the high resolution surface, (C) low resolution 5 × 5 µm^2 and (D) rolling ball image.

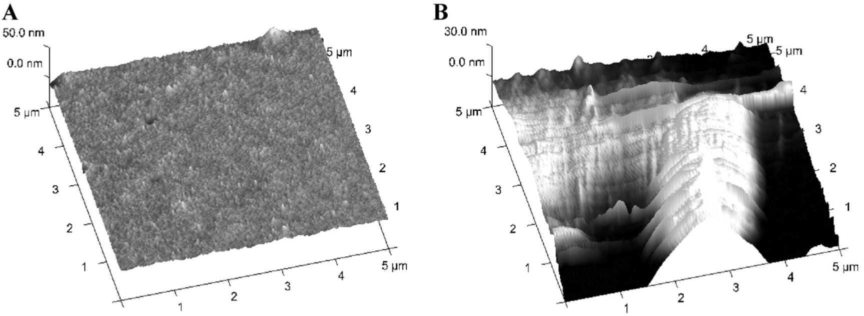

Figure 5. Surfaces covered with silanized silica particles (A) 9 nm high resolution 5 × 5 µm^2 and (B) 9 nm low resolution 5 × 5 µm^2.

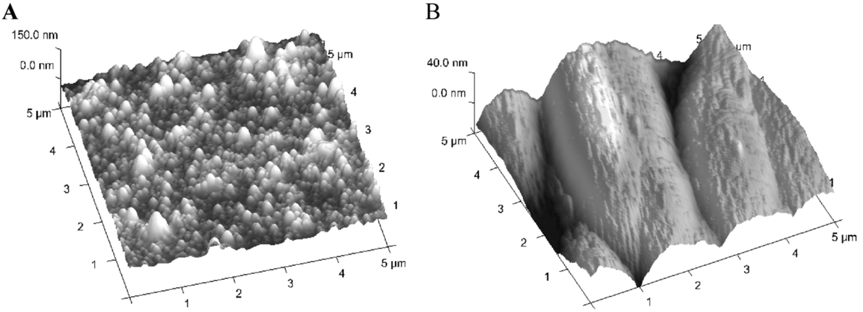

Figure 6. Surfaces covered with silanized silica particles (A) 40 nm high resolution $5 \times 5\ \mu m^2$ and (B) 40 nm low resolution $5 \times 5\ \mu m^2$.

Table 2. Roughness characteristics and water contact angle of nanoparticle-coated and silanized silica substrates.

Sample	R_a *(nm)*	R_q *(nm)*	*Water contact angle*
9 nm	1.42	2.84	85°
40 nm	13.1	17.6	91°

3.2 Surface interactions

The force measurements over the $5 \times 5\ \mu m^2$ area were conducted at 25 different spots in the order illustrated in Figure 7. This pattern was chosen in order to avoid any artificial regularity in the force map due to accumulation of air, for example, at the force measuring spot. The force maps shown in Figure 8 contain two data sets extracted from the 540 force curves obtained on each surface and used to create the images. Figures 8A, 8C and 8E illustrate how the jump-in distance varies over the surface region for the surfaces polished for 2 s, 10 s and 40 s, respectively. The jump-in distance corresponds to the surface separation at which the gradient of the attractive force just exceeds the spring constant of the cantilever, and is a measure of the range of the attraction. The strength of the attraction in contact is determined from the jump-out distance during separation, and these data sets are shown in the adhesion maps illustrated in Figures 8B, 8D and 8F. The force maps illustrated in Figure 8 can be directly compared with the low-resolution images in Figures 2C, 3C and 4C. We note that the clear patterns seen in the

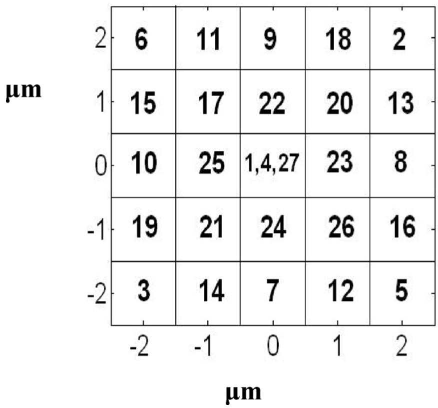

	-2	-1	0	1	2
2	6	11	9	18	2
1	15	17	22	20	13
0	10	25	1,4,27	23	8
-1	19	21	24	26	16
-2	3	14	7	12	5

Figure 7. Force measurement order.

topographical images are not reflected in the force maps, and we conclude that the large-scale waviness of the surface does not significantly affect the forces, but the range and magnitude of the attraction appear to vary randomly over the surfaces.

The variation in jump-in distance and adhesion force as a function of force measurement number for the surfaces polished for 2 s, 10 s and 40 s are shown in Figure 9. In all cases we note a significantly larger difference between spots on the surface than between measurements on one and the same spot, providing clear evidence that the local topography, rather than the large-scale waviness, has an effect on the measured force. Neither the adhesion force nor the jump-in distance shows any discernible trend with the number of measurements.

The jump-in distance and adhesion histograms obtained for the polished surfaces are illustrated in Figure 10. In all cases a distribution of values is obtained, with a width that is significantly larger for the surface polished for 2 s compared to that found for the more smooth surfaces obtained after further polishing. The average value for the adhesion and the jump-in distance are also decreasing with increasing polishing time, i.e. with decreasing surface roughness, see Table 3.

The corresponding data for the nanoparticle coated surfaces are reported in Table 4. The spread in these values is larger, in terms of absolute values, for the surface with the smaller nanoparticles but the CV is larger for the surface coated with larger nanoparticles. When comparing the data for the two different nanoparticle coated surfaces, we note that the attraction is more

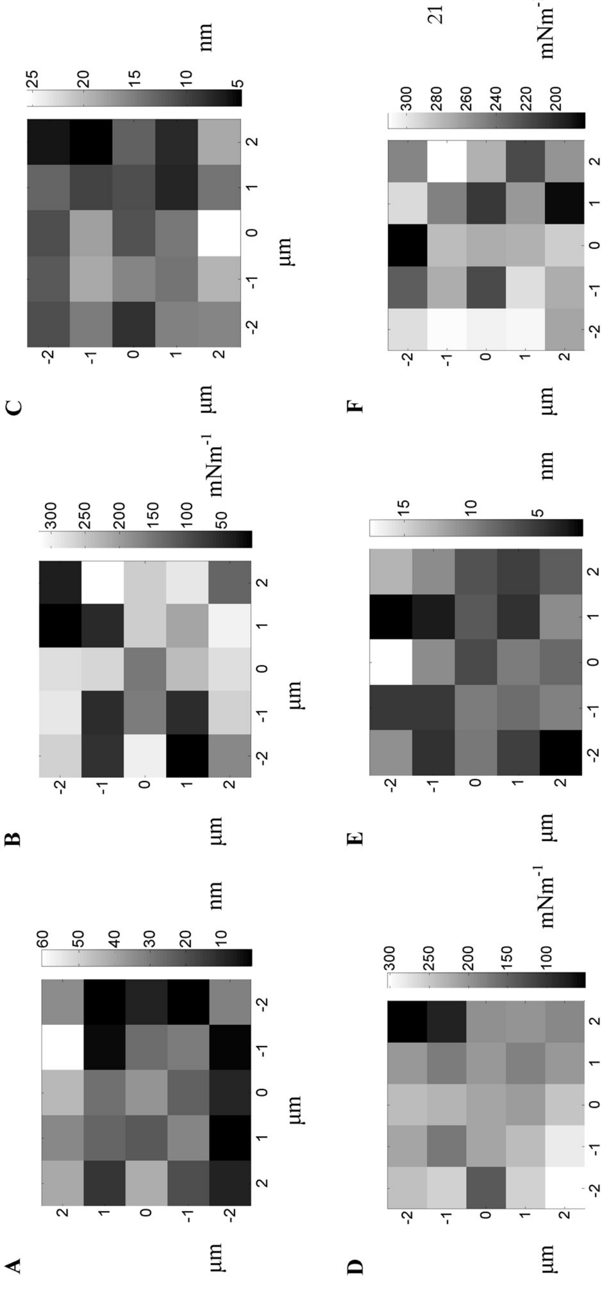

Figure 8. Force maps over 5 × 5 μm^2 polished surfaces. (A) 2 s jump-in distance, (B) 2 s adhesion, (C) 10 s jump-in distance (D) 10 s adhesion, (D) 40 s jump-in distance (E) 40 s adhesion.

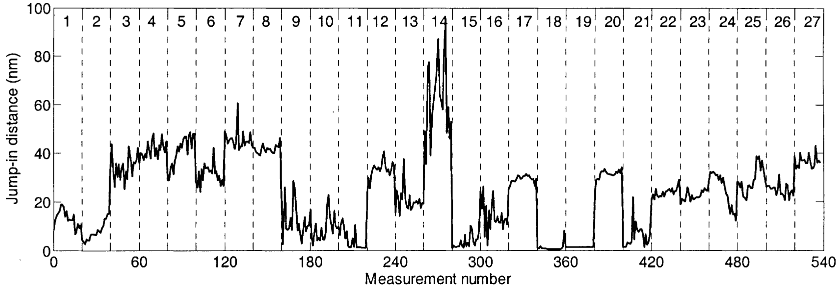
Jump-in distance (nm)
0
20
40
60
80
100
Measurement number
0
60
120
180
240
300
360
420
480
540
1 2 3 4 5 6 7 8 9 10 11 12 13 14 15 16 17 18 19 20 21 22 23 24 25 26 27

A

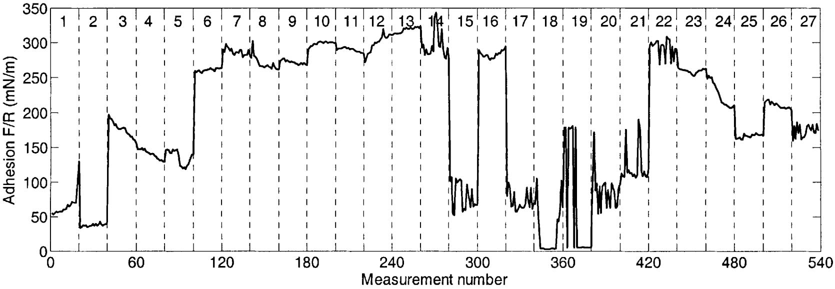
Adhesion F/R (mN/m)
0
50
100
150
200
250
300
350
Measurement number
0
60
120
180
240
300
360
420
480
540
1 2 3 4 5 6 7 8 9 10 11 12 13 14 15 16 17 18 19 20 21 22 23 24 25 26 27

B

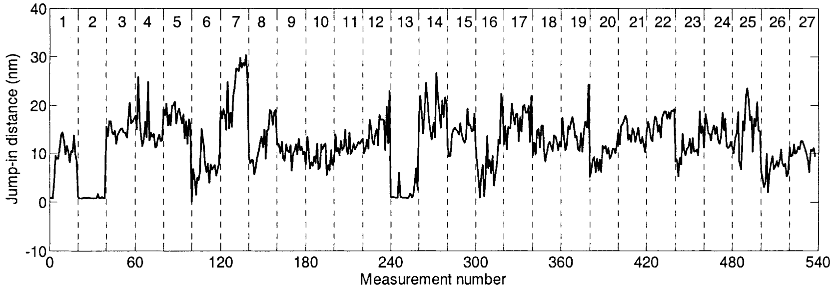
Jump-in distance (nm)
-10
0
10
20
30
40
Measurement number
0
60
120
180
240
300
360
420
480
540
1 2 3 4 5 6 7 8 9 10 11 12 13 14 15 16 17 18 19 20 21 22 23 24 25 26 27

C

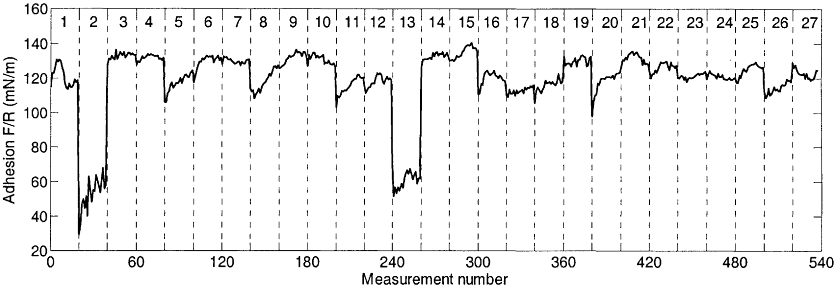
Adhesion F/R (mN/m)
20
40
60
80
100
120
140
160
Measurement number
0
60
120
180
240
300
360
420
480
540
1 2 3 4 5 6 7 8 9 10 11 12 13 14 15 16 17 18 19 20 21 22 23 24 25 26 27

D

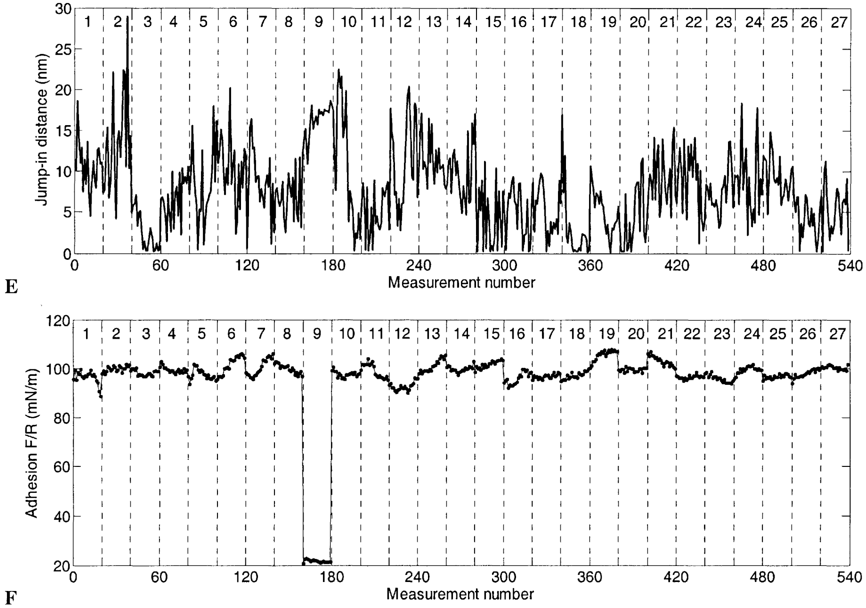

Figure 9. Force as a function of measurement number frequencies for polished surfaces. (A) 2 s jump-in distance, (B) 2 s adhesion, (C) 10 s jump-in distance, (D) 10 s adhesion, (E) 40 s jump-in distance, (F) 40 s adhesion.

Table 3. Adhesion and jump-in distance for surfaces polished for different times. The scatter is given as standard deviations and coefficients of variation, CV.

	2 s	*10 s*	*40 s*
Adhesion			
Mean value (mNm^{-1})	188	124	98
Standard deviation (mNm^{-1})	103	20	14
CV (%)	55	16	14
Jump-in distance			
Mean value (nm)	24	13	8
Standard deviation (nm)	16	5	5
CV (%)	67	38	62

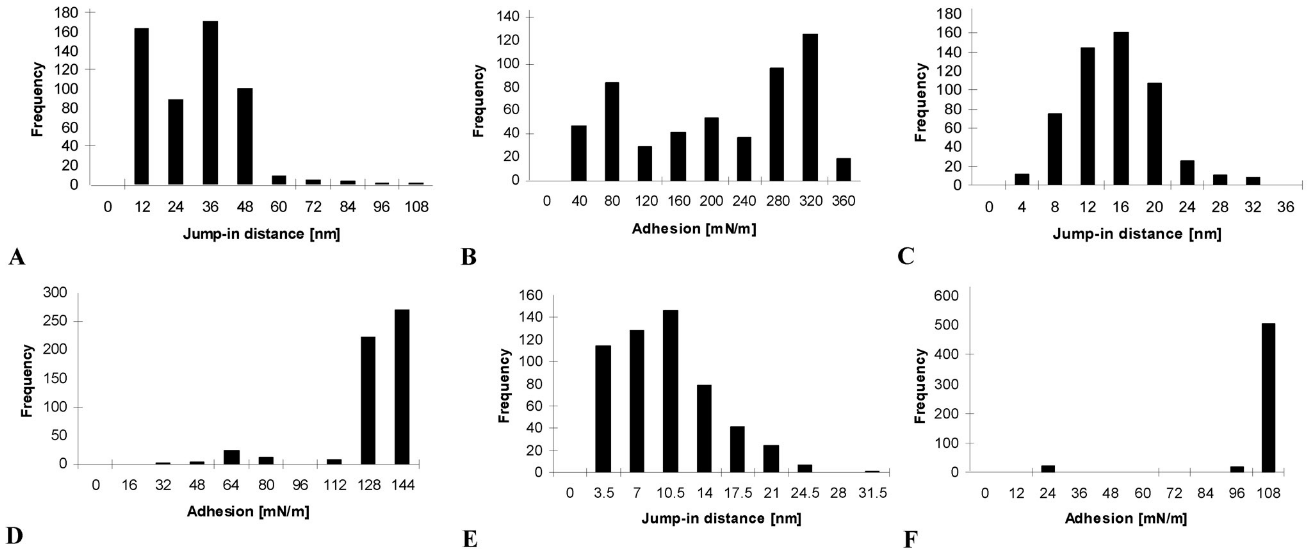

Figure 10. Force frequencies for polished surfaces. (A) 2 s jump-in distance, (B) 2 s adhesion, (C) 10 s jump-in distance, (D) 10 s adhesion, (E) 40 s jump-in distance and (F) 40 s adhesion.

Table 4. Adhesion and jump-in distance. The scatter is given as standard deviations and coefficients of variation, CV.

	9 nm	*40 nm*
Adhesion		
Mean value (mNm^{-1})	83	8
Standard deviation (mNm^{-1})	23	7
CV (%)	28	88
Jump-in distance		
Mean value (nm)	31	9
Standard deviation (nm)	10	9
CV (%)	32	100

long-ranged and the adhesion is higher for the surface with the smaller nanoparticles even though the macroscopic contact angle is lower on this surface.

Examples of force curves measured on approach and on separation are provided in Figure 11. We note that on approach the attraction sets in suddenly once a critically small distance has been reached. This defines the jump-in distance, which is larger than expected for a van der Waals force. On separation a strong adhesion is observed. In strongly attractive regions the jump-out occurs directly to zero force, whereas in less strongly attractive regions a long-range attraction is noted on separation (see Figure 11C). This attraction approaches zero rapidly once a critically large distance is reached.

These features are qualitatively explained as follows: at the jump-in distance an air/vapour cavity forms between the surfaces and an attractive Laplace pressure brings them together. On separation the cavity is extended until it becomes unstable and disappears, at which point the force returns to zero. We note that for the polished surfaces a repulsion is present prior to the jump-in. This feature is suggested to be due to an initial deformation of a surface bound bubble, a description consistent with others [20–23]. As the bubble bursts, and a capillary condensate of air/vapour is formed between the surfaces, a strong capillary attraction is developed.

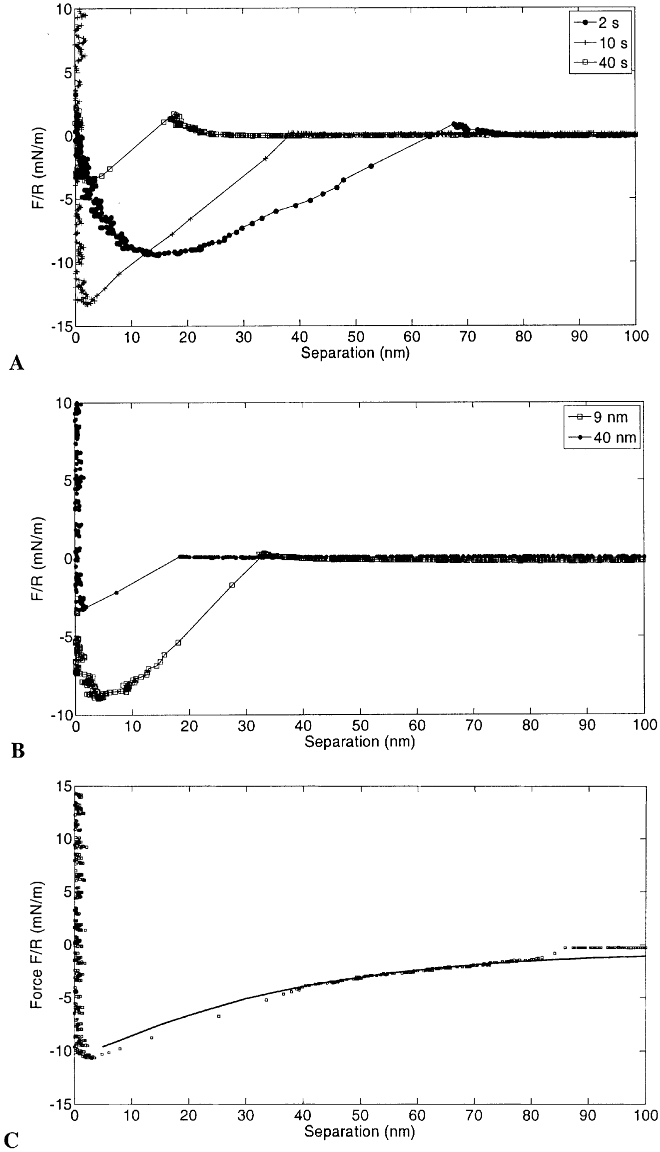

Figure 11. (A) Force on approach versus distance for surface polished 2 s (dots), 10 s (squares) and 40 s (crosses). (B) Force on approach versus distance for surface covered with 9 nm silanized silica particles (squares) and 40 nm silanized silica particles (dots). (C) [see opposite page] Separation versus distance for surface covered with 40 nm silanized silica particles. Solid line represents theoretical capillary condensation.

4. DISCUSSION

4.1 Adhesion between rough surfaces

The adhesion force, F_{adh}, between a sphere, with radius R, and a flat surface is related to the interfacial energy as:

$$\frac{F_{adh}}{R} = \alpha(\gamma_{sl} - \gamma_{sls}) \tag{1}$$

where α is a constant with a value between 3π and 4π, depending on surface radius and elasticity of the contacting bodies [24–26]. The quantity γ_{sl} is the interfacial energy between the solid and the liquid and γ_{sls} is the excess free energy associated with the contact. This latter quantity approaches zero for atomically flat surfaces whereas it approaches the value of γ_{sl} for very rough surfaces. Since rough surfaces were used in this study, meaning that the real contact area is small, the adhesion as described by eq. [1] is also small. (Note that the adhesion force by convention is regarded as a positive value, whereas the attractive forces displayed in the force curves by convention are given a negative sign).

The long-range force due to the presence of a capillary condensate, with a volume that does not change with separation, is approximately given by [27, 28]:

$$\frac{F}{R} = 4\pi\gamma_{lv}\cos\theta\left[1 - \frac{1}{\sqrt{1 + d^2/D^2}}\right] \tag{2}$$

where D is the surface separation, d a constant related to the size of the capillary condensate and θ is the contact angle of the vapour/air cavity (i.e. 180° – the local water contact angle) on the surface. This equation describes the long-range attraction observed during separation, as shown in Figure 11C. Thus, a cavity is present between the surfaces during separation, and this cavity will contribute to the measured adhesion force.

The vapour cavity contribution to the adhesion arises from the Laplace pressure, and it is given by the second term in eq. [3] [29]:

$$\frac{F_{adh}}{R} = \alpha(\gamma_{sl} - \gamma_{sls}) + 4\pi\gamma_{lv}\cos\theta \tag{3}$$

where γ_{lv} is the water-vapour surface energy. We note that measurements of macroscopic water contact angles on the rough surfaces used in this investigation are in the range 85–93°.

If we assume that the first term in eq. [3] is negligibly small compared to the second one, we can then estimate the contact angles of the cavity from the adhesion force. For instance, for the surfaces polished for 2 s, the mean adhesion force, 188 mNm^{-1}, corresponds to a contact angle of the capillary condensate of 78°, and within the standard deviation shown in Table 3, this angle varies in the range 71–85°. The corresponding values for the surface polished for 10 s are 82° for the mean value, and within one standard deviation of the adhesion force the contact angle varies between 81° and 85°. Thus, the large variation in adhesion force can readily be assigned to small differences in vapour contact angle. We note that if the direct adhesion between the surfaces, i.e. the first term in eq. [3], is not negligible, then the contact angle of the cavity would be even closer to 90° than indicated by this analysis.

One fundamental assumption in the treatment above is that the cavity is allowed to grow to its optimum size. This is a reasonable assumption for flat and homogeneous surfaces, as also indicated by experiments [2]. However, this is not obvious when considering cavities formed on rough and chemically non-homogeneous surfaces where pinning of the three phase line may occur, in analogue to the contact angle hysteresis observed on the macroscopic level. To illustrate the consequences of this, we turn to the treatment of capillary condensation by Wennerström *et al.* [27]. The free energy change due to formation of a capillary condensate of air is given by:

$$\Delta G = A_{s1}(\gamma_{s1v} - \gamma_{s1l}) + A_{s2}(\gamma_{s2v} - \gamma_{s2l}) + A_{lv}\gamma_{lv} + V_c\Delta\mu \tag{4}$$

where the first two terms are due to the free energy change of replacing a surface-water interface, of area A_{s1} and A_{s2} on the two surfaces, with a surface-vapour interface. The sum of these two terms has to be sufficiently negative for a cavity to form. The third term is due to the free energy cost of creating an air-water interface with area A_{lv}, and the fourth term is due to the difference in chemical potential, μ, between water vapour and air present in the cavity with volume V_c, and water and dissolved air in the surrounding aqueous phase. Thus, if the three-phase line is pinned and the cavity is prevented from growing to its optimal size, then the free energy gain is reduced. The adhesion force is given by:

$$F_{adh} = \left(\frac{\partial\Delta G}{\partial D}\right)_{D=0} \tag{5}$$

In the cylindrical approximation the relevant areas and volume are given as $A_{s1} = A_{s2} = \pi R_m^2$, $A_{lv} = 2\pi R_m D$, and $V_c = \pi R_m^2 D$, where R_m is the cylinder radius. This immediately gives:

$$\frac{F_{adh}}{R} = \frac{2\pi R_m \gamma_{lv}}{R} + \frac{\pi R_m^2 \Delta\mu}{R} \tag{6}$$

This relation, which is valid beyond the cylindrical cavity approximation [27], shows that the adhesion force also decreases when the cavity is prevented from growing to its optimal size due to pinning of the three-phase line. This is suggested to be another reason for the variation in adhesion values observed in this investigation.

4.2 Comparison between nanostructured surfaces with 9 nm and 40 nm particles

The range and magnitude of the attraction is larger for the surface with smaller nanoparticles, despite that this surface is slightly less hydrophobic as judged from contact angle measurements. This allows us to draw the conclusion that macroscopic contact angle measurements cannot be used for predicting the range of capillary forces between nanostructured surfaces. Our data rather show that a capillary condensate of air/vapour forms more easily when the nanoscale roughness is smaller. There are at least two effects that contribute to this. Firstly, the crevices formed on the surface are larger when larger nanoparticles are used, providing a larger volume for gas accumulation at the surface. Secondly, the growth of the capillary is hampered by the increased nanoscale roughness since the three-phase line has to move over larger surface features as the capillary grows. This is akin to the well-known effect of surface roughness on macroscopic contact angle hysteresis. The adhesion is also higher when smaller nanoparticles are used to build the nanostructure. This is suggested also to be a consequence of the pinning of the three-phase line, which leads to smaller cavities and/or contact angles closer to 90° on the surface with larger nanoscopic features.

4.3 Comparison between nanostructured surfaces and polished surfaces

The polished surfaces have some small surface features that extend away from the surface, but unlike the case of nanostructured surfaces they largely lack nanoscopic crevices. Thus, air that accumulates at the surface cannot concentrate in any crevices, but must rather exist as a thin film or as nanobubbles. For the polished surfaces a repulsive force is nearly always preceding the onset of the capillary attraction, providing strong evidence for the presence of nanobubbles on these surfaces. This is in clear contrast to the results for the nanostructured surfaces, where this feature was not observed. The adhesion forces observed for the polished surfaces were larger than those measured for the nanostructured surfaces, indicating that the relatively few topographical peaks do not hamper the growth of the capillary to the same extent as the dense topographical features of the nanostructured surfaces. Surprisingly, for the polished surfaces we note the highest adhesion and most long-range attraction for the roughest surface. This leads to the conclusion that these extended surface features promote the formation of air/vapour capillary condensates, presumably by stabilizing the adsorbed nanobubbles.

5. CONCLUSIONS

Surfaces with nanometre scale roughness have been prepared by (a) by polishing silica surface and (b) by spin-coating of nanometre sized silica particles onto unpolished silica surfaces. After silanation these surfaces display macroscopic contact angles of close to 90°. For both types of surfaces a capillary attraction dominates the interaction with a hydrophobized probe particle.

The polished surfaces have surface texture displaying sharp extended surface features separated by relatively smooth regions without any crevices. On these surfaces, preadsorbed nanobubbles are suggested to be present and a soft repulsion due to electrostatic repulsion and bubble deformation precedes the capillary attraction on approach. In contrast, the spin-coated surfaces display a nanostructure with crevices and ridges due to the individual nanoparticles. Both type of surfaces also display a waviness over larger length scales, comparable to the size of our probe particle. Our force data show that the large-scale waviness has no significant influence of the range or magnitude of the capillary force. The range and magnitude of this force does, however, vary significantly at different spots on the surface. The large variation in adhesion force can be attributed to a small variation in the local contact angle between the air/vapour capillary and the surfaces. The pinning of the three-phase line is suggested to contribute to this variation and also to hamper the growth of the capillary condensate to its equilibrium size. Despite that the nanostructured surface with larger surface features (40 nm particles) displays a larger macroscopic contact angle than that of the nanostructured surface with smaller features (9 nm particles), the range and magnitude of the capillary attraction is larger in the latter case. This is interpreted as being due to less severe restrictions to capillary growth on the surface with smaller nanostructures.

Taken together, our data suggest that the presence of a high density of nanoscopic crevices on the surface reduces the range and magnitude of the capillary attraction due to accumulation of air in these crevices. Contrary, the presence of extended nanoscopic surface features, as for the polished surfaces, stabilizes nanobubbles and enhances the capillary attraction.

6. ACKNOWLEDGEMENTS

Omya Development AG is thanked for funding this project and for supporting cooperation between YKI and its industrial Mineral and Surface Chemistry R&D. Silvan Fischer at Omya Development AG is thanked for performing the polishing work. Funding was also provided through Research Institutes of Sweden (RISE Holding AB, formerly IRECO Holding AB) for VW and AS. PMC acknowledges financial support from the Swedish Research Council (VR).

7. REFERENCES

1. J.N. Israelachvili and R.M. Pashley. Measurement of the Hydrophobic Interaction between Two Hydrophobic Surfaces in Aqueous Electrolyte Solutions. *Journal of Colloid and Interface Science* 98(2):500–514, 1984.
2. H.K. Christenson and P.M. Claesson. Cavitation and the Interaction between Macroscopic Hydrophobic Surfaces. *Science* 239(4838):390–392, 1988.
3. J.L. Parker and P.M. Claesson. Bubbles, Cavities, and the Long-Ranged Attraction between Hydrophobic Surfaces. *Journal of Physical Chemistry* 98:8468–8480, 1994.
4. A. Carambassis, Jonker, L. C., Attard, P., Rutland, M. W. Forces Measured between Hydrophobic Surfaces Due to a Submicroscopic Bridging Bubble. *Physical Review Letters* 80:5357–5360, 1998.
5. T. Ederth, P.M. Claesson and B. Liedberg. Self-Assembled Monolayers of Alkanethiols on Thin Gold Films as Substrates for Surfaces Force Measurements. Long-Range Hydrophobic Interactions and Electrostatic Double-Layer Interactions. *Langmuir* 14:4782–4789, 1998.
6. H.K. Christenson and P.M. Claesson. Direct Measurements of the Force between Hydrophobic Surfaces in Water. *Advances in Colloid and Interface Science* 91:391–436, 2001.
7. P. Luckham. Manipulating Forces between Surfaces: Applications in Colloid Science and Biophysics. *Advances in Colloid and Interface Science* 111:29–47, 2004.
8. J.C. Fröberg, O.J. Rojas and P.M. Claesson. Surface Forces and Measuring Techniques. *International Journal of Mineral Processing* 56:1–30, 1999.
9. E.E. Meyer, K.J. Rosenberg and J.N. Israelachvili. Recent Progress in Understanding Hydrophobic Interactions. *Proceedings of the National Academy of Sciences of the United States of America* 103(43):15739–15746, 2006.

10. S. Yang, S.M. Dammer, N. Bremond and H.J.W. Zandvliet. Characterization of Nanobubbles on Hydrophobic Surfaces in Water. *Langmuir* 23:7072–7077, 2007.
11. B.M. Borkent, S.M. Dammer, H. Schönherr, G.J. Vancso and D. Lohse. Superstability of Surface Nanobubbles. *Physical Review Letters* 98:204502–204501 – 204502–204504, 2007.
12. E. Thormann, A.C. Simonsen, P.L. Hansen and O.G. Mouritsen. Interactions between a Polystyrene Particle and Hydrophilic and Hydrophobic Surfaces in Aqueous Solutions. *Langmuir* 24(14):7278–7284, 2008.
13. A.V. Nguyen, J. Nalaskowski, J.D. Miller and H.-J. Butt. Attraction between Hydrophobic Surfaces Studied by Atomic Force Microscopy. *International Journal of Mineral processing*:215–225, 2003.
14. M. Hato. Attractive Forces between Surfaces of Controlled "Hydrophobicity" across Water: A Possible Range of "Hydrophobic Interactions" between Macroscopic Hydrophobic Surfaces across Water. *J. Phys. Chem.* 100:18530–18538, 1996.
15. V. Wallqvist, P.M. Claesson, A. Swerin, J. Schoelkopf and P.A.C. Gane. Interaction Forces between Talc and Hydrophobic Particles Probed by AFM. *Colloids and Surfaces A* 277(2–3):183–190, 2006.
16. V. Wallqvist, P.M. Claesson, A. Swerin, J. Schoelkopf and P.A.C. Gane. Interaction Forces between Talc and Pitch Probed by Atomic Force Microscopy. *Langmuir* 23(8):4248–4256, 2007.
17. J. Iruthayaraj, E. Poptoshev, A. Vareikis, R. Makiska and A. Van Der Wal. Adsorption of Low Charge Density Polyelectrolyte Containing Poly(Ethylene Oxide) Side Chains on Silica: Effects of Ionic Strength and Ph. *Macromolecules* 38:6152–6160, 2005.
18. J.E. Sader, J.W.M. Chon and P. Mulvaney. Calibration of Rectangular Atomic Force Microscope Cantilevers. *Review of Scientific Instruments* 70(10):3967–3969, 1999.
19. M. Axelsson, C. Östlund, H. Vomhoff and S. Svensson. Estimation of the Pore Volume at the Interface between Paper Web and Press Felt. *Nordic Pulp and Paper Research Journal* 21(3):395–402, 2006.
20. P. Attard. Nanobubbles and the Hydrophobic Attraction. *Advances in Colloid and Interface Science* 104(1–3):75–91, 2003.
21. J. Mahnke, J. Stearnes, R.A. Hayes, D. Fornasiero and J. Ralston. The Influence of Dissolved Gas on the Interactions between Surfaces of Different Hydrophobicity in Aqueous Media Part I. Measurement of Interaction Forces. *Phys. Chem. Chem. Phys.* 1:2793–2798, 1999.
22. J.W.G. Tyrell and P. Attard. Images of Nanobubbles on Hydrophobic Surfaces and Their Interactions. *Physical Review Letters* 87:1761041–1761044, 2001.
23. J.W.G. Tyrell and P. Attard. Atomic Force Microscope Images of Nanobubbles on a Hydrophobic Surface and Corresponding Force-Separation Data. *Langmuir* 18:160–167, 2002.
24. K.L. Johnson, K. Kendall and A.D. Roberts. Surface Energy and the Contact of Elastic Solids. *Proceedings of the Royal Society of London A* 324:301–313, 1971.

25. B.V. Derjaguin, V.M. Muller and Y.P. Toporov. Effect of Contact Deformations on the Adhesion of Particles. *Journal of colloid and interface science* 53(2):314–326, 1975.
26. J.L. Parker and P. Attard. Deformation of Surfaces Due to Surface Forces. *Journal of Physical Chemistry* 96:10398–10405, 1992.
27. P. Petrov, U. Olsson and H. Wennerström. Surface Forces in Biocontinous Microemulsion: Water Capillary Condensation and Lamellae Formation. *Langmuir* 13(13):3331–3337, 1997.
28. E. Blomberg, Claesson, P. M., Wärnheim, T. Surface Interactions in Emulsions and Liposome Solutions. *Colloids and Surfaces A: Physiochemical and Engineering Aspects* 159:149–157, 1999.
29. H.K. Christenson. Capillary Condensation in Systems of Immiscible Liquids. *Journal of colloid and interface science* 104(1):234–249, 1984.

Transcription of Discussion

ADHESIVE AND LONG-RANGE CAPILLARY FORCES BETWEEN HYDROPHOBIC SURFACES IN WATER: EFFECTS OF SURFACE TOPOGRAPHY

Viveca Wallqvist,[1] *Per M. Claesson*,[1,2] *Agne Swerin*,[1]
Catherine Östlund,[3] *Joachim Schoelkopf*[4] and
Patrick A.C. Gane[4,5]

[1]YKI, Ytkemiska Institutet AB/Institute for Surface Chemistry, Box 5607, SE-114 86 Stockholm, Sweden
[2]Department of Chemistry, Surface and Corrosion Science, Royal Institute of Technology, SE-100 44 Stockholm, Sweden
[3]Innventia AB, Box 5604, SE-114 86 Stockholm, Sweden
[4]Omya Development AG, CH-4665 Oftringen, Switzerland
[5]Department of Forest Products Technology, Helsinki University of Technology, FI-02015 Helsinki, Finland

Gil Garnier Australian Pulp and Paper Institute

Thank you, Agne – beautiful work. I am trying to visualize hydrophobic forces having a longer range than the van der Waals forces, and to help me to understand that I have two related questions. The first one is, does the hydrophobic force increase with the hydrophobicity of the surface? If you go from polyethylene to Teflon do you see an increase in this hydrophobic component?

Agne Swerin

Yes, we do. But it is also combined with – which is probably the second question – the introduction of structural features on the surface.

Gil Garnier

No. My second question was, if you decrease the polarity of the fluid by, for example, introducing methanol or propanol into the water contained in the cell, do you see a decrease of this force?

Agne Swerin

The answer is yes. We investigated that as one part of the PhD project where we were looking at wetting and dispersing additives.

Lars Wågberg KTH

Thank you, Agne, for a clear and nice presentation with interesting results. I wonder, in the cavity model (according to Eq. 2), when you did the fitting, which radius did you use?

Agne Swerin

That is the radius of the probe.

Lars Wågberg

But is it not a bit more complex than that? If you look at the bubble formation, the force that you create when the cavity is formed, is naturally related to some fraction of the radius of the probe, but it must be also related to the structure on the surface.

Agne Swerin

Yes, in this case you have the radius of the probe, R, you have the surface distance, D, and you have d which is a constant related to the size of the capillary condensate, so that includes the effect of the surface features.

Lars Wågberg

Thank you.

Janet Preston Imerys Minerals

Thank you for the presentation. Please could you tell us any more about the impact of dispersion aids in your work? You just mentioned that you did work with dispersants; what were your findings?

Agne Swerin

We used one wetting agent and one dispersing agent and both are needed to prepare talc dispersions to be used in the paper industry. We saw a clear difference between these in how they behave when it comes to maintaining, or even taking away, the long-range interaction. A wetting agent would, in this case, lower the surface tension in the system, and take away much of the long-range interaction. We noted that this wetting agent apparently did not adsorb onto the surface, it adhered to the air-vapour cavities being formed, and reduced the long-range interaction. But when we went back to pure water, we got back the long-range interaction. For the dispersing agent we did not see this happening. A point worth mentioning is that we measured adhesion forces between a probe and a talc platelet surface. One of the speculations for how wetting and dispersing agents work, specifically for talc, is that you have an attraction both to the planes of the talc and to the edges and, in this particular set-up, we could not measure the interaction with the edges.

Bob Pelton McMaster University,

Long-range attractive forces between hydrophobic surfaces have been observed for many years, and in the early days there was a lot of argument over the mechanism. I have not followed this literature closely. Are we absolutely sure that it is little air bubbles holding these things together, is there no doubt about that now?

Agne Swerin

We strongly believe that this is the only way to explain what we see in terms of experiments. We have seen this now in so many different types of experimental system. The new thing about this work is that we could measure the effect in talc-pitch systems and we have extended that to these more detailed surface features. One reason why we did this was to explain why, in particular, talc but also other hydrophobic materials can be very good at adsorbing sticky contaminants.